Journal of Molecular Catalysis A: Chemical 344 (2011) 11–17

Contents lists available at ScienceDirect

Journal of Molecular Catalysis A: Chemical

journal homepage: www.elsevier.com/locate/molcata

Review

Water gas shift reaction over Zn–Ni/SiO_2 catalyst prepared from $[Zn(H_2O)_6]_2[Ni(NCS)_6]\cdot H_2O/SiO_2$ precursor

Ali Reza Salehi Rad, Maryam behzad khoshgouei, Ali Reza Rezvani*

Department of Chemistry, University of Sistan and Baluchestan, P. O. Box 98135-674, Zahedan, Iran

ARTICLE INFO

Article history:
Received 3 December 2010
Received in revised form 8 March 2011
Accepted 7 April 2011
Available online 22 April 2011

Keywords:
Novel precursor
$[Zn(H_2O)_6]_2[Ni(NCS)_6]\cdot H_2O/SiO_2$
Bimetallic catalyst
Complex
Water gas shift reaction

ABSTRACT

Silica-supported Zn–Ni catalyst prepared by thermal decomposition of $[Zn(H_2O)_6]_2[Ni(NCS)_6]\cdot H_2O/SiO_2$ precursor was tested in the water gas shift reaction. The characterization of both precursor and calcined catalyst was carried out using powder X-ray diffraction (XRD), FT-infrared, scanning electron microscopy (SEM), BET specific surface area and thermal analysis methods (TGA and DSC). The water gas shift reaction was studied over prepared catalyst in the temperature range of 280–420 °C, gas hourly space velocity (GHSV) of 3600 h^{-1} and H_2O/CO molar ratio of 4 at atmospheric pressure. The Zn–Ni/SiO_2 catalyst presented higher activity than the reference catalysts prepared by impregnation and co-precipitation methods.

Contents

* Corresponding author. Tel.: +98 541 245 2337; fax: +98 541 244 3388.
E-mail address: rezvani2001ir@yahoo.ca (A.R. Rezvani).

1381-1169/$ – see front matter © 2011 Elsevier B.V. All rights reserved.
doi:10.1016/j.molcata.2011.04.010

1. Introduction

The water gas shift (WGS) reaction ($CO + H_2O \leftrightarrow CO_2 + H_2$) is an important step in several industrial processes [1,2]. It is used to increase the hydrogen production and remove CO before ammonia synthesis, refinery hydroprocesses and redistribution of hydrogen, or to adjust the H_2/CO ratio in the methanol production and the Fischer–Tropsch synthesis [3,4].

The WGS reaction is also investigated widely in fuel cell technology because of its potential for high fuel efficiency and lower emissions [5,6].

The water gas shift (WGS) reaction is moderately exothermic, being thermodynamically limited at high temperatures. Nevertheless, high temperatures are required to increase the reaction rate. Therefore, the WGS reaction is performed in two stages with different temperature regions. The first step (high temperature shift, HTS) is typically operated at 310–450 °C using Fe–Cr based catalysts and the second stage (low temperature shift, LTS) is approximately operated at the temperature between 180 and 250 °C with Cu–Zn based catalysts [7,8]. Ni catalyst has been also investigated to ascertain its suitability for the WGS [2].

The method of catalyst preparation plays an important role in the physical properties and catalytic performance of the catalysts. In previous researches, Zn/Ni oxide catalysts were prepared by co-precipitation [9,10], urea hydrolysis [11,12], citrate sol–gel [13] and incipient wetness impregnation [14] methods. In this paper, the results obtained with Zn-promoted Ni/SiO_2 catalyst prepared by thermal decomposition of $[Zn(H_2O)_6]_2[Ni(NCS)_6]\cdot H_2O/SiO_2$ precursor are reported.

This method potentially provides many advantages as a preparative route since: (a) the use of inorganic precursor complexes enables materials having well defined metal loadings to be achieved, (b) the intimate metal contact within the inorganic complex can be retained, thereby ensuring homogeneous dispersion of the metals onto the support, (c) synergetic metal–metal or metal–metal oxide interactions which improve catalytic performance, and (d) many inorganic complexes contain metals in low oxidation states and decomposition enables, pre-reduced, metals to be obtained, facilitating the use of milder catalyst activation conditions. Therefore, this preparation method is an ideal technique for the preparation of materials containing two (or more) metallic or oxide phases.

2. Experimental

2.1. Materials

All the chemicals and solvents were regent grade. The water was distilled and deionized. $Ni(NO_3)_2\cdot 6H_2O$, $Zn(NO_3)_2\cdot 6H_2O$, SiO_2 and NH_4SCN were purchased from Aldrich.

2.2. Preparation of $[Zn(H_2O)_6]_2[Ni(NCS)_6]\cdot H_2O$

An aqueous solution (5 mL) of NH_4SCN (0.457 g, 6 mmol) was added to a solution of $Ni(NO_3)_2\cdot 6H_2O$ (0.29 g, 1 mmol) in water (10 mL), and the mixture was stirred at room temperature for 5 h. To this solution was then added $Zn(NO_3)_2\cdot 6H_2O$ (0.595 g, 2 mmol) and the resulting solution was stirred at room temperature for 1 h. The final solution was filtered and left for slow evaporation in air. Air-stable and water-soluble crystals were obtained in ca. 65%. Anal. Calc. for $C_6H_{26}N_6Zn_2O_{13}S_6Ni$ (772.1 g): C, 9.33; H, 3.37; N, 10.88. Found: C, 9.12; H, 3.29; N, 10.82%. IR (KBr, cm^{-1}): 3440, 3200, 2090, 1610, 825, 610, 472. UV–Vis (H_2O, nm): 218, 272, 400, 674, 740. Λ_M (H_2O) = 262 $ohm^{-1}\,cm^2\,mol^{-1}$.

2.3. Preparation of $[Zn(H_2O)_6]_2[Ni(NCS)_6]\cdot H_2O/SiO_2$ precursor

To a solution containing $[Zn(H_2O)_6]_2[Ni(NCS)_6]\cdot H_2O$ (10 mmol, 7.72 g) in 100 mL water was added SiO_2 (600 mg), and the mixture was stirred and evaporated at 30 °C to dryness.

2.4. Preparation of silica-supported zinc–nickel catalyst, $Zn–Ni/SiO_2$

The $[Zn(H_2O)_6]_2[Ni(NCS)_6]\cdot H_2O/SiO_2$ precursor was calcined at 600 °C in static air in the electric furnace for 4 h. The grey powder, $Zn–Ni/SiO_2$ was formed and kept in desicator.

2.5. Preparation of reference catalysts

For comparative purposes, the $Zn–Ni/SiO_2$ reference catalysts were prepared by impregnation and co-precipitation methods. In the co-precipitation method, the required quantity of silica was added to an aqueous solution of nickel nitrate ($Ni(NO_3)_2\cdot 6H_2O$) and zinc nitrate ($Zn(NO_3)_2\cdot 6H_2O$) (1:2) and mixture was stirred for several hours to obtain homogeneity. Subsequently, a Na_2CO_3 solution was added to this mixture. PH was simultaneously, controlled by dropping an aqueous solution of NaOH at room temperature. The precipitate was dried at 120 °C and finally calcined at 600 °C for 4 h. In the impregnation method, silica was impregnated with an aqueous solution of nickel nitrate and zinc nitrate, for 24 h. After drying overnight at 120 °C, the precursor catalyst was calcined at 600 °C for 4 h.

2.6. Catalyst characterization

2.6.1. X-ray diffraction (XRD)

XRD patterns were recorded on a FK60-04 diffractometer between 5° and 70° (2θ) with a step size 0.02 using Cu Kα radiation. Diffraction patterns were assigned using the PDF database supplied by the international centre for diffraction data (PDF2-Diffraction Database File).

2.6.2. Scanning electron microscopy (SEM)

Scanning electron microscopy (SEM) studies were conducted using a Jeol JSM 5410 microscope, operating with an accelerating voltage of 10 kV.

2.6.3. Brunauer–Emmett–Teller (BET) surface area measurements

The BET surface areas and pore volumes were measured with the nitrogen physisorption at −196 °C using a Quantachrome NOVA 4200e apparatus. Each sample was degassed under vacuum at 300 °C for 3 h prior to the measurement.

2.6.4. Elemental analysis, conductometric, FT-IR, UV–Vis, and atomic absorption spectroscopy

Elemental analysis was performed on a Perkin-Elmer 2400 CHNS/O elemental analyzer. Conductivity reading was obtained using a Ciba Corning model check-mate 90 conductivity meter. IR spectra (4000–400 cm^{-1}) were measured on a FT-IR JASCO 460 spectrophotometer with KBr pellets. UV–Vis spectroscopy was performed on a JASCO 7850 spectrophotometer. The atomic absorption spectroscopy on metals was carried out by using a Varian AA50 equipment.

2.6.5. Thermal gravimetric analysis (TGA)

The weight changes of catalyst precursor were recorded by using TGA-PL England equipment. The sample, ca. 15 mg, was placed in a Pt cell and heated from room temperature to 600 °C at a heating rate of 10 °C min^{-1} with a gas feed (Ar) of 50 mL min^{-1}.

2.6.6. Differential scanning calorimetry (DSC)

DSC was performed on a NETZSCH DSC 200 F3, with a heating rate of 10 °C min^{-1} under a flow of dry air.

2.7. Catalyst testing

Catalytic tests under CO/H_2O were performed in a fixed bed microreactor (i.d. 3 mm) operating at atmospheric pressure. The reaction temperature was controlled by a thermocouple inserted into catalyst bed. The catalyst (1.0 g) was reduced in situ at atmospheric pressure in a flowing H_2–N_2 stream (N_2/H_2 = 1, flow rate of each gas = 30 mL min^{-1}) at 400 °C for 6 h prior to reaction. Then the N_2/H_2 was replaced by the H_2O/CO (4:1) mixture with a GHSV of 3600 h^{-1}. The water gas shift reaction was carried out between 280 and 420 °C, 8 h for each temperature. The inlet and outlet gas was product steams were analyzed on line using a gas chromatograph (Varian, Model 3400 series) equipped with a 10-port sampling valve (Supelco company, USA, Visi Model), a sample loop and a thermal conductivity detector. The performance of the catalyst was evaluated in terms of two parameters:

$$\text{CO conversion} = \frac{(F_{CO,in} - F_{CO,out})}{F_{CO,in}} \quad \text{(I)}$$

where $F_{CO,in}$ and $F_{CO,out}$ represent the molar flow of the CO species measured at the inlet and at the outlet of the reactor, respectively.

$$\text{CO}_2 \text{ selectivity} = \frac{F_{CO_2}}{F_T} \quad \text{(II)}$$

where F_{CO_2} and F_T are the molar flow of the carbon dioxide and total molar flow of the products (methane and carbon dioxide), respectively.

3. Results and discussion

3.1. Complex characterization

The bimetallic complex, $[Zn(H_2O)_6]_2[Ni(NCS)_6]$, was synthesized by reaction of $[Zn(H_2O)_6]^{2+}$ with $[Ni(NCS)_6]^{4-}$ at room temperature (298 K). The molecular ion, $[Ni(NCS)_6]^{4-}$, was generated in solution by addition of six moles of ammonium thiocyanate to one mole of nickel (II) nitrate hexahydrate in water. The complementary unit $[Zn(H_2O)_6]^{2+}$ was produced in an aqueous solution of zinc (II) nitrate hexahydrate 2M. The details of the sequential reactions are summarized in Eqs. (1) and (2).

$$Ni(NO_3)_2{\cdot}6H_2O + 6NH_4NCS \rightarrow (NH_4)_4[Ni(NCS)_6] + 2NH_4NO_3 + 6H_2O \quad (1)$$

$$(NH_4)_4[Ni(NCS)_6] + 2[Zn(H_2O)_6](NO_3)_2 \rightarrow [Zn(H_2O)_6]_2[Ni(NCS)_6] + 4NH_4NO_3 \quad (2)$$

In the infrared spectrum of the $[Zn(H_2O)_6]_2[Ni(NCS)_6]{\cdot}H_2O$ complex, the thiocyanate C–N stretching frequency is observed as a very strong band at 2090 cm^{-1}. Its position and rather broad nature are characteristic of N-bonded thiocyanate. The C=S stretching mode of free SCN^- (749 cm^{-1}) is shifted to higher frequency (825 cm^{-1}) in the corresponding complex which is consistent with nitrogen bonding to the nickel. The absorption band at 472 cm^{-1} is assigned to N–C–S bending mode and it affords further confirmation that thiocyanate groups are N-bonded. In S-bonded complexes this vibration occurs between 440 and 410 cm^{-1} and is split into several components [15,16].

The strong and broad band in 3440–3520 cm^{-1} region is attributable to the ν(OH) stretching vibrations which indicates the presence of coordinated water. The sharp and weak absorption band at 3200 cm^{-1} and a sharp band at 1610 cm^{-1} are assigned to crystallization water molecules in the crystal lattice. The weak band at 610 cm^{-1} is assigned to the Ni–N stretching vibration in complex. This stretching vibration mode is attributed to the coordination of –NCS to the nickel.

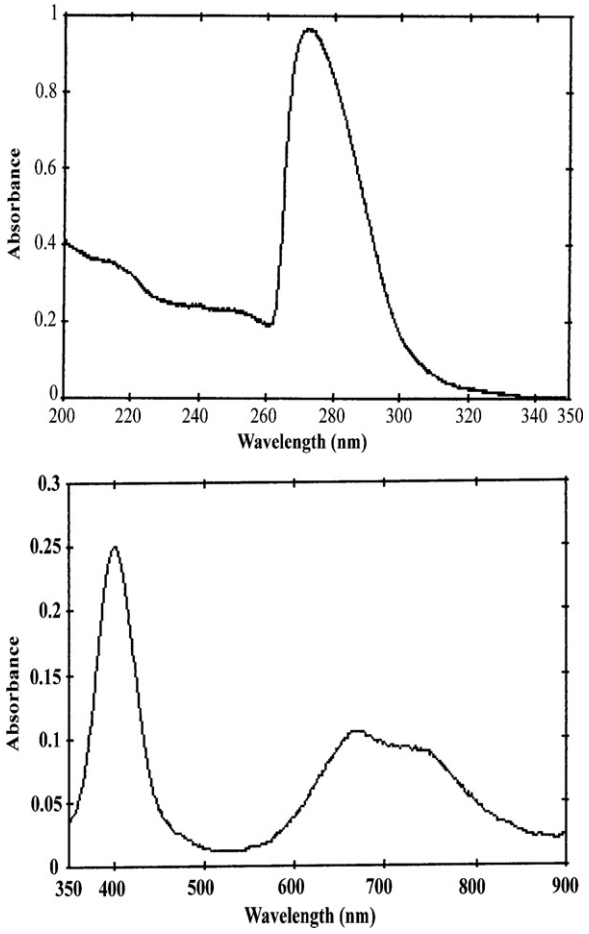

Fig. 1. Electronic spectra of $[Zn(H_2O)_6]_2[Ni(NCS)_6]{\cdot}H_2O$.

The presence in molar ratio of 2:1 Zn^{II}/Ni^{II} in the complex is corroborated by atomic absorption spectroscopy analysis which gives satisfactory values for those metals.

Fig. 1 shows the electronic spectra of the complex in H_2O. The electronic spectrum in UV region exhibits absorption bands at 218 and 272 nm for the complex attributed to intra-ligand $n \rightarrow \pi^*$ and $\pi \rightarrow \pi^*$ transitions, respectively. The absorption bands at 400, 674 and 740 nm are almost coincident with those reported for transitions $^3A_{2g}(F) \rightarrow {}^3T_{1g}(p)$ and $^3A_{2g}(F) \rightarrow {}^3T_{1g}(F)$ in octahedral Ni^{2+} species, the band due to $^3A_{2g}(F) \rightarrow {}^3T_{1g}(F)$ transition being split by spin-orbit coupling.

The molar conductivity value for an aqueous solution of $[Zn(H_2O)_6]_2[Ni(NCS)_6]{\cdot}H_2O$ complex (Λ_M = 262 ohm^{-1} cm^2 mol^{-1}) suggests that it forms a 2:1 electrolyte in water and dissociates to give the cationic $[Zn(H_2O)_6]^{2+}$ and the anionic $[Ni(NCS)_6]^{4-}$ species, respectively.

3.2. Characterization of catalyst and its precursor

In the IR spectrum of the calcined catalyst, the absorption band at 445 cm^{-1} and the shoulder at 580 cm^{-1} are assigned to the transverse optical (TO) fundamental and the longitudinal (LO) modes of NiO, respectively [17]. The absorption bands at 407 (TO) and 570 cm^{-1} (LO) are attributed to crystalline ZnO [18]. The typical absorption bands of pure silica are also observed.

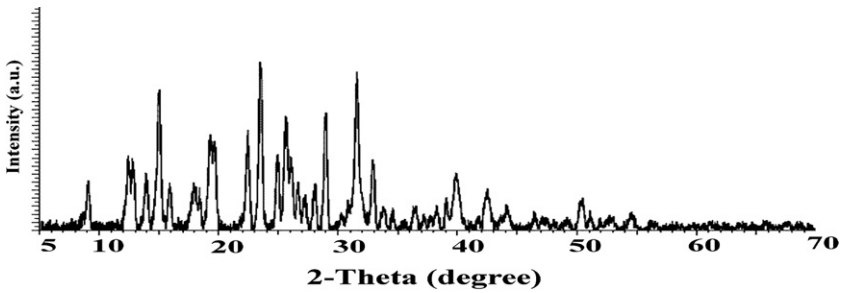

Fig. 2. Powder X-ray diffraction pattern of precursor.

Table 1
Textural properties of the precursor, Zn–Ni/SiO_2 and reference catalysts.

Sample	BET surface area (m^2/g)	Pore volume (cm^3/g)	d_{NiO} (nm)	d_{ZnO} (nm)
$[Zn(H_2O)_6]_2[Ni(NCS)_6]\cdot H_2O/SiO_2$	9.7	0.14		
Zn–Ni/SiO_2	163.6	0.49	5.3	12.1
Reference catalyst (imp)	132.2	0.38	16.6	26.2
Reference catalyst (cop)	115.4	0.29	17.9	26.9

Fig. 2 shows the XRD pattern of the precursor. The diffraction lines of precursor (at 2θ = 14.9, 19.6, 22.4, 23.4, 23.7, 25.8, 28.9 and 31.6°) are of high intensity and of low half-width, which are typical of well-crystallized sample. The XRD patterns for the calcined catalyst prepared from novel precursor and the calcined reference catalysts prepared by impregnation and co-precipitation are presented in Fig. 3. All the samples exhibit the characteristic XRD peaks of NiO (at 2θ = 37.2, 43.2 and 62.8°) and ZnO (at 2θ = 31.7, 34.3, 36.2, 47.5, 56.5 and 67.8°). The absence of any type of reflection that could be assigned to silicates indicates that there is no apparent interaction between the Zn–Ni catalyst and the SiO_2 support. The characteristic peaks of NiO and ZnO in Zn–Ni/SiO_2 catalyst are broader than those in reference catalysts, suggesting that preparation method of Zn–Ni/SiO_2 catalyst can promote the dispersion of NiO and ZnO and make their crystallite size smaller. The crystallite sizes of NiO and ZnO were calculated from NiO (2 0 0) and ZnO (1 1 0) by the Scherrer equation (Table 1). The smallest crystallite sizes (NiO and ZnO) were observed over the prepared Zn–Ni/SiO_2 catalyst and the largest over the reference catalyst prepared by co-precipitation. The XRD pattern of the reduced catalyst (Fig. 4) exhibits characteristic peaks for metallic Ni (at 2θ = 44.5 and 51.8°), ZnO (at 2θ = 31.7, 34.3, 36.2, 47.5, 56.5 and 67.8°) and Zn–Ni alloy (at 2θ = 43.6, 44.3 and 51.2°).

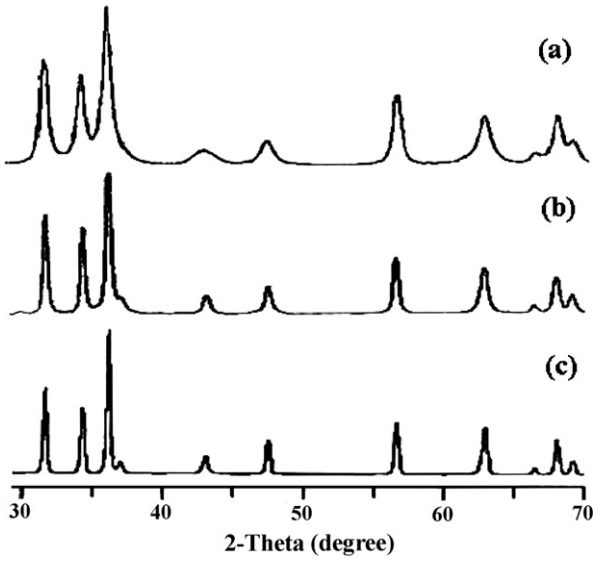

Fig. 3. Powder X-ray diffraction patterns of (a) calcined Zn–Ni/SiO_2 catalyst and calcined reference catalysts prepared by (b) impregnation, and (c) co-precipitation.

The precursor, $[Zn(H_2O)_6]_2[Ni(NCS)_6]\cdot H_2O/SiO_2$, was characterized by thermal gravimetric analysis (TGA), to indicate decomposition of $[Zn(H_2O)_6]_2[Ni(NCS)_6]\cdot H_2O$ complex (Fig. 5). The TGA data for precursor shows three steps weight loss. The first stage, a weight loss over 80–110 °C, corresponds to the removal of lattice water molecule. The second stage, abrupt weight loss in the region 120–230 °C, is due to the loss of coordinated water molecules. Six thiocyanate ions are decomposed in the third stage above 250 °C. The weight loss continued up to 600 °C and the final decomposition products were the stable oxides forms, identified by IR spectroscopy.

Differential scanning calorimetry (DSC) curve for the precursor exhibits one endothermic peak and five exo-effects (Fig. 6). The endothermic peak between 80 and 110 °C is assigned to the removal of the crystal water molecule. Two exothermic peaks in the region 200–320 °C are attributed to crystallization of ZnO and

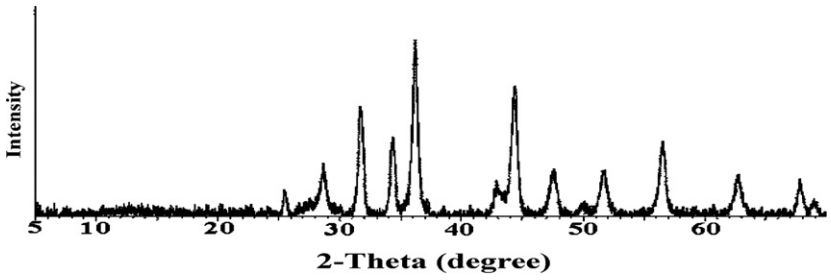

Fig. 4. Powder X-ray diffraction pattern of reduced catalyst.

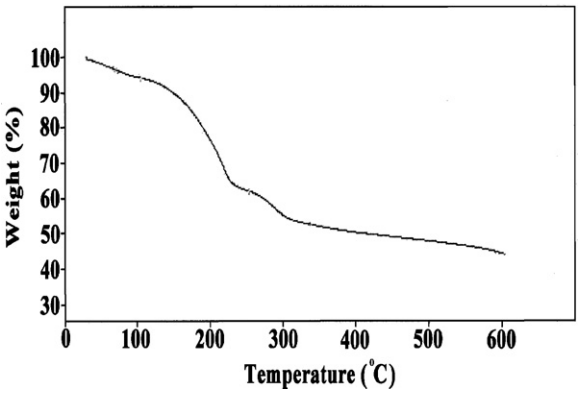

Fig. 5. Thermogram of $[Zn(H_2O)_6]_2[Ni(NCS)_6]\cdot H_2O/SiO_2$ precursor.

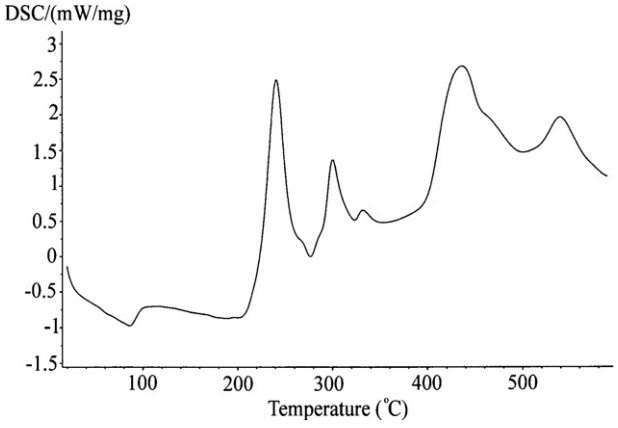

Fig. 6. DSC curve for the $[Zn(H_2O)_6]_2[Ni(NCS)_6]\cdot H_2O/SiO_2$ precursor.

NiO phases. (The presence of these phases has been established by X-ray diffraction measurements as well.) Three exothermic peaks in the temperature interval from 320 to 580 °C are probably due to the burning of the thiocyanate ligands.

Characterization of both precursor and calcined catalyst was also carried out using scanning electron microscopy (SEM). All the electron micrographs were obtained from powder specimens of these materials. SEM observations (Fig. 7) have shown differences in morphology of both precursor and calcined catalyst. The electron micrograph obtained from catalyst precursor (Fig. 7a) depicts several agglomerations of crystalline particles. This is an agreement with XRD pattern which showed the crystalline phase. The morphological features of calcined catalyst (Fig. 7b) are quite different

Table 2
Influence of reaction temperature on catalytic performance of the Zn–Ni/SiO_2 catalyst in the water gas shift (WGS) reaction.

Temperature (°C)	CO_2 selectivity (%)	CH_4 selectivity (%)
280	99.0	1.0
300	98.7	1.3
320	96.9	3.1
340	95.7	4.3
360	92.3	7.7
380	90.9	9.1
400	90.3	9.7
420	90.2	9.8

H_2O/CO molar ratio: 4, GHSV: 3600 h^{-1}, 1.0 g of catalyst.

with the precursor and show that the agglomerate size is greatly decreased in compared to the precursor sample described above.

Textural properties of the precursor, calcined catalyst and reference catalysts are shown in Table 1. As shown in Table 1, the BET surface area and pore volume of the precursor are very low, about 9.7 m^2/g and 0.14 cm^3/g, respectively. It can be seen that after calcination, both the BET surface area and pore volume greatly increased to 163.6 m^2/g and 0.49 cm^3/g, respectively. The occurrence of high surface area for calcined catalyst can be attributed to the preparation method adopted (thermal decomposition of $[Zn(H_2O)_6]_2[Ni(NCS)_6]\cdot H_2O/SiO_2$ precursor) and, also, to the use of silica support [19]. With increasing the amount of SiO_2, the BET surface area increases [20]. The results of BET specific surface area of prepared catalyst are in good agreement with SEM observation, which showed the agglomerate size of the calcined catalyst is less than its precursor and therefore, leads to an increase in the BET specific area of the calcined sample. The specific surface area of the prepared catalyst is larger than the specific surface areas of the reference catalysts. This shows improved dispersion of the NiO active phase, which is beneficial for the performance of the catalyst.

3.3. Catalytic tests

3.3.1. Effect of temperature

The water gas shift reaction over the Zn–Ni/SiO_2 catalyst was carried out at atmospheric pressure in the temperature range of 280–420 °C and at a gas hourly space velocity (GHSV) of 3600 h^{-1}. The H_2O/CO ratio was kept constant at 4:1 for all the experiments. Table 2 shows the effect of temperature on water gas shift reaction in terms CO_2 selectivity and methane selectivity. The effect of reaction temperature on CO conversion of prepared catalyst is shown in Fig. 8. For comparison, the equilibrium CO conversion and CO conversions of reference catalysts are also presented in Fig. 8.

It can be seen, that with increasing temperature from 300 to 420 °C, the CO conversion decreased from 96.5% to 89.2%. Furthermore, it can be observed that with increasing temperature from

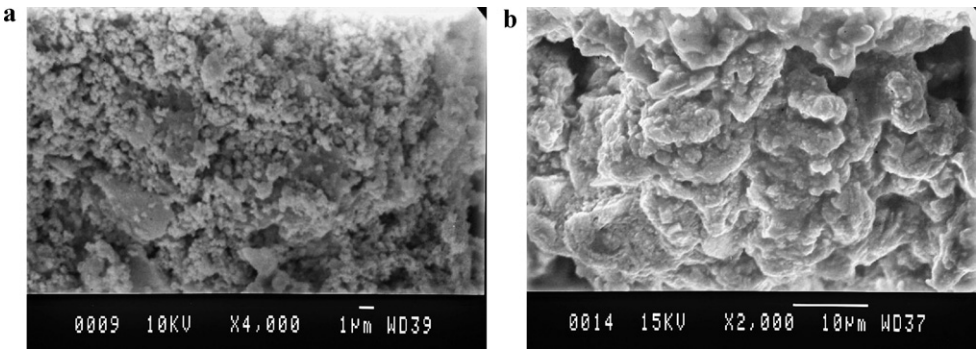

Fig. 7. SEM micrographs of: (a) precursor, and (b) calcined catalyst.

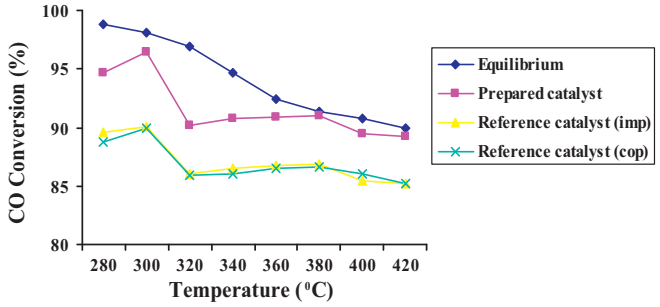

Fig. 8. Effect of reaction temperature on CO Conversion of Zn–Ni/SiO_2 and reference catalysts in the water gas shift reaction.

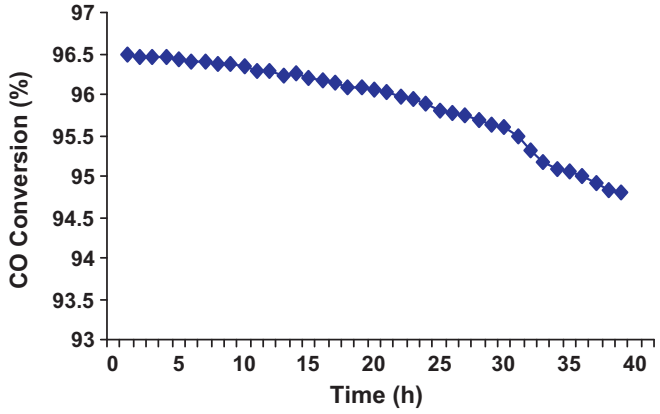

Fig. 9. Stability performances of Zn–Ni/SiO_2 catalyst at 300 °C.

320 to 380 °C the CO conversion slightly increased from 90.2% to 91%. At higher temperature, 400 and 420 °C, the CO conversion is reduced to 89.5% and 89.2%, respectively. Water gas shift reaction is a moderately exothermic reaction in nature; therefore, from Le chatelier's principle it is known that the reaction tends to shift to the left side at high temperatures. This leads to a lower CO conversion. Alternatively, seeing that the reaction rate or Arrhenius law is temperature-dependent, an increase in CO conversion will be exhibited as the reaction temperature is lifted [21].

With increasing temperature, CO_2 selectivity decreased due to methane produced by methanation.

The catalyst exhibits the maximum catalytic performance at 300 °C. Therefore, the water gas shift reaction on Zn–Ni/SiO_2 catalyst is investigated at 300 °C (a medium temperature) in this work.

The Zn–Ni/SiO_2 catalyst has higher activity compared to the reference catalysts prepared by impregnation and co-precipitation conventional methods. The higher catalytic activity of Zn–Ni/SiO_2 is mainly related to chemical properties, instead of physical structures. Compared with the results obtained for reference catalysts higher surface area and smaller crystallite size can be ascribed to the different preparation methods and preparation parameters.

3.3.2. Stability test

Stability performance was performed over Zn–Ni/SiO_2 catalyst at 300 °C, at temperature which CO conversion reach the maximum. Fig. 9 shows the profile of CO conversion versus time. The catalytic activity of Zn–Ni/SiO_2 was stable for 10 h. The CO conversion decreases by 1.7% during the 40 h test. In the spent catalyst, the BET measurements indicated that the specific surface area of Zn–Ni/SiO_2 catalyst was decreased from 144.7 to 137.2 m^2/g. During the 40 h test at 300 °C, the Ni dispersion was also decreased from 23.2% to 21.6% and this is considered to be the reason for the deactivation for this catalyst after long time of operation. The stability test for reference catalysts showed that both samples were stable during the 10 h test (Fig. 10).

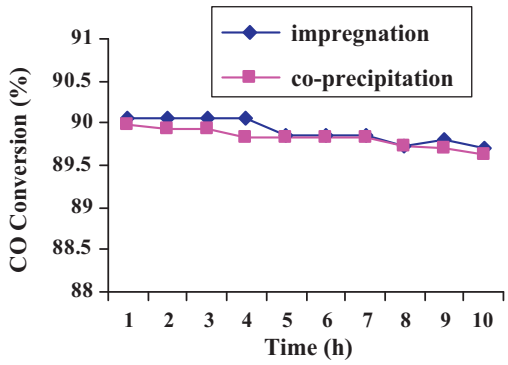

Fig. 10. CO conversion of reference catalysts at 300 °C as a function of time.

4. Conclusions

The Zn–Ni/SiO_2 catalyst prepared by thermal decomposition of a new precursor, $[Zn(H_2O)_6]_2[Ni(NCS)_6]\cdot H_2O/SiO_2$. This method is a simple and suitable way to preparation of supported binary catalysts for different catalytic processes. Combining the results of the FT-IR spectra, TGA/DSC curves, classical identification method, and XRD patterns for $[Zn(H_2O)_6]_2[Ni(NCS)_6]\cdot H_2O$ complex, precursor, and calcined catalyst showed the complex decomposed to form nickel and zinc oxides as the solid products and a mixture of carbon, nitrogen and sulfur oxides as gaseous products.

Comparison between the surface area of this Zn–Ni catalyst and other supported zinc–nickel catalysts show a higher surface area for the present catalyst [9–14,22]. As attested by value of BET specific surface area, the preparation method (thermal decomposition of Zn–Ni bimetallic complex) allows obtaining a highly dispersed solid.

The catalytic tests at 280–420 °C (P = 1 atm, $H_2O/CO = 4:1$) showed that the Zn–Ni/SiO_2 catalyst has the high catalytic activity for water gas shift (WGS) reaction. The prepared catalyst presented higher activity than the reference catalysts prepared by impregnation and co-precipitation methods. The higher activity of this catalyst can be attributed to the higher surface area and smaller ZnO and NiO particle sizes.

Acknowledgement

The authors are grateful to the USB for financial support.

References

[1] P. Liu, J.A. Rodriguez, Y. Takahashi, K. Nakamura, J. Catal. 262 (2009) 294–303.
[2] Y. Li, Q. Fu, M. Flytzani - Stephanopoulos, Appl. Catal. B: Environ. 27 (2000) 179–191.
[3] F. Huber, J. Walmsley, H. Venvik, A. Holmen, Appl. Catal. A: Gen. 349 (2008) 46–54.
[4] T.R. Oliveira de Souza, S.M.O. Brito, H.M.C. Andrade, Appl. Catal. A: Gen. 178 (1999) 7–15.
[5] C. Zerva, C.J. Philippopoulos, Appl. Catal. B: Environ. 67 (2006) 105–112.
[6] X. Qi, M. Flytzani - Stephanopoulos, Ind. Eng. Chem. Res. 43 (2004) 3055–3062.
[7] C. Martos, J. Dufour, A. Ruiz, Int. J. Hydrogen Energy 34 (2009) 4475–4481.
[8] M. Marono, J.M. Sanchez, E. Ruiz, Int. J. Hydrogen Energy 35 (2010) 37–45.
[9] N. Homs, J. Llorca, P.R. Piscina, Catal. Today 116 (2006) 361–366.
[10] X. Deng, J. Sun, S. Yu, J. Xi, W. Zhu, X. Qiu, Int. J. Hydrogen Energy 33 (2008) 1008–1013.
[11] G. Busca, U. Costantino, T. Montanari, G. Ramis, C. Resini, M. Sisani, Int. J. Hydrogen energy 35 (2010) 5356–5366.
[12] C. Resini, T. Montanari, L. Barattini, G. Ramis, G. Busca, S. Presto, P. Riani, R. Marazza, M. Sisani, F. Marmottini, U. Costantino, Appl. Catal. A: Gen. 355 (2009) 83–93.

[13] M.N. Barroso, M.F. Gomez, L.A. Arrua, M.C. Abello, Appl. Catal. A: Gen. 304 (2006) 116–123.
[14] A. Denis, W. Grzegorczyk, W. Gac, A. Machocki, Catal. Today 137 (2008) 453–459.
[15] K. Nakamoto, Infrared and Raman Spectra of Inorganic and Coordination Compounds, 5th ed., Wiley-Interscience, New York, 1997.
[16] P.F. Raphel, E. Manoj, M.R.P. Kurup, Polyhedron 26 (2007) 818–826.
[17] S. Mochizuki, Phys. Status Solidi B 126 (1984) 105–114.
[18] J.M. Calleja, M. Cardona, Phys. Rev B 16 (1977) 3753–3761.
[19] B.M. Reddy, G.M. Kumar, I. Ganesh, A. Khan, J. Mol. Catal. A: Chem. 247 (2006) 80–87.
[20] Y. Yang, H.W. Xiang, L. Tian, H. Wang, C.H. Zhang, Z.C. Tao, Y. Yxu, B. Zhong, Y.W. Li, Appl. Catal. A: Gen. 284 (2005) 105–122.
[21] W. Chen, M. Lin, T.L. Jiang, M. Chen, Int. J. Hydrogen energy (2008) 6644–6656.
[22] C.F. Linares, J. Lopez, A. Scaffidi, C.E. Scott, Appl. Catal. A: Gen. 292 (2005) 113–117.